Probing Phase Transformations and Microstructures at the Small Scales - Synchrotron X-Ray Microdiffraction for Advanced Applications in Phase Change Memory, 3D IC (Integrated Circuits) and Solar PV (Photovoltaics) Devices

I. Radchenko, S. K. Tippabhotla, N. Tamura, A.S. Budiman

Abstract

Local crystal orientation, lattice distortion and phase transformations can all be probed using submicron size x-ray beam and Laue diffraction. Fast data collection provided by state-of-the-art area detectors at synchrotron facilities and new pattern indexing algorithms optimized for speed make it possible to map large portions of a sample in a reasonable amount of time and get quantitative images of its microstructure in near real time. This technique is particularly suitable for studying the mechanical and microstructural properties of inhomogeneous multi-phase polycrystalline samples. A recent development is Laue diffraction phase mapping which provides quantitative phase distribution in complex crystalline materials. This article will explore the recent developments in that respect at the Advanced Light Source, illustrated with a few advanced applications in the microelectronics, phase-change memory and solar PV devices/systems and propose as the underlying theme, the technique's unique capability to unravel insights that are otherwise not possible or at least impractical to obtain otherwise, and thus enabling the next generation of devices/systems.

1 Introduction

X-ray diffraction (XRD) is a well-known technique to study the crystalline structure of materials. Synchrotron X-ray microdiffraction (μXRD), as is used on Beamline 12.3.2 of the Advanced Light Source (ALS), Lawrence Berkeley National Lab [Tamura et al. (2009)], adds high spatial resolution to a standard, laboratory-scale XRD technique by utilizing the orders of magnitude higher intensity of polychromatic (white) beam synchrotron source and submicron focused X-ray beam. The schematic of synchrotron μXRD is shown on Fig. 1.

The use of a polychromatic x-ray source in combination with a 2D detector open the ability to obtain quickly a set of x-ray reflections without a need to rotate the sample, via the collection of a Laue pattern. The typical Laue pattern of a polycrystalline sample is shown on Fig. 2. From the Laue pattern, one can identify the crystal structure of the material, calculate the crystal rotation matrix and deviatoric strain/stress tensor, characterize the plastic deformation in the material including the density of geometrically necessary dislocations [Tamura (2014)].

White beam from synchrotron source can be filtered to become monochromatic, using a monochromator allowing to generate more conventional XRD patterns. They can be used to obtain the hydrostatic strain/stress, which gives the complete strain/stress state of the material after obtaining the deviatoric components from the corresponding Laue pattern.

Another feature of synchrotron μXRD is a high energies (short wavelengths) of X-rays, allowing to penetrate into a material without a need to destroy/take out the surface layers.

Since X-ray beam can be focused to a submicron size, synchrotron μXRD can be used to characterize the crystalline structures at submicron resolution and provide very rich and unprecedented information about the crystal microstructure, how it deviates from its theoretical state (i.e. stresses and strains, defects, such as dislocations, grain boundaries, etc.) and perhaps more importantly how it evolves during operations and/or mechanical/electrical loading of advanced devices and systems in the technologically important areas such as microelectronics and energy applications. [Budiman et al. (2009)-Budiman et al. (2015)]. This article is intended to provide a summary of how this technique has been utilized on Beamline 12.3.2 at the ALS, Berkeley Lab, and subsequently provided unique, hitherto not known (or at least, very difficult or not practical to obtain) insights into not only how to build robust and reliable advanced devices [Budiman et al. (2009)-Chen et al. (2008)] but also to enable higher performance and to allow novel design for next generation, lower cost systems [Budiman et al. (2014); Budiman et al. (2012); Rengarajan et al. (2016); Tippabhotla et al. (2016)]. It is our hope that by providing the summary of three seemingly unrelated advanced applications in one integrated comparison/survey study, the article could more vividly provide the underlying theme and thus unraveling deeper insights into the capabilities of the technique and its potential uses in many other areas.

In this article, we present advanced applications of the technique in three technologically important areas:

- Study of the crystallization kinetics of phase change memory materials
- Study of the stress state in 3D microelectronic chips
- Study of the reliability of thin $c-Si$ solar PV for next generation energy systems

For all the studies, the capabilities of synchrotron μXRD at Beamline 12.3.2 (Advanced Light Source, Lawrence Berkeley Lab, CA, USA) were used. While the special experimental set up for each of the studies will be summarized in the following sections, many of the common beamline/end-station instrumental setup of the Beamline 12.3.2 has been described and comprehensively summarized elsewhere [Tamura et al. (2009)].

2 Probing Advanced Phase Change Memory Materials

Phase change materials exhibit a reversible transformations between crystalline and amorphous phases due to the change in temperature [Kolobov et al. (2007); WeŃnic and Wuttig (2008)]. In some cases, electrical or optical properties of such materials changes drastically during phase transformation [Kolobov et al. (2004)-Lencer et al. (2008)]. These effects are used to design modern information storage devices [Raoux and Ielmini (2009); Lencer et al. (2011)]. The operation of such devices strongly depends on crystallization kinetics. Hence, it is important to understand the factors, influencing the crystallization kinetics of phase change materials.

Here, we summarize how we had used the unique strength of the synchrotron technique, i.e. its non-destructive abilities to characterize the crystalline structure of the phase change memory (PCM) materials and study how it actually evolves from its crystalline state to its amorphous one (*in situ*) and as such very quantitative information, otherwise not known (or very difficult/impractical to obtain) about the kinetics of the phase transformation [Sutou et al. (2012); Svoboda and Málek (2011)], which is in the very essence of how this advanced memory device works, was actually obtained in report studies of the crystallization kinetic of sputtered amorphous *GeTe* films (1μm thick) as a function of deposition temperature and deposition rate [Khoo et al. (2016)].

In this study two sets of *GeTe* films were deposited using RF-magnetron sputtering. *Si* coated with thin layer of native was used as a substrate. *Ar* pressure during sputtering was maintained at Torr. First set of the films was deposited with a deposition rate of 8nm/min at room temperature, 60, 80 and 100. The second set of samples was deposited at room temperature with a deposition rates of 7.1nm/min, 8.8nm/min and 10.3nm/min by varying *Ar* gas pressure. The amorphous films than heated up from the room temperature to 235, where they exhibit a full crystallization which is clear from its XRD pattern (see Figure Error: Reference source not found). The crystallization was studied using monochromatic beam in synchrotron μXRD. Transformation curves where obtained by tracking the intensity of (011) *GeTe* peak during the annealing. The effective activation energies for the crystallization where calculated from the transformation curves using Kissinger's analysis [Kissinger (1957)].

The effect of deposition temperature is shown on Fig. 4. It is clear that the activation energy of nucleation is decreasing at higher deposition temperatures. The activation energy of growth is not affected by the deposition temperature. It is also not affected by the deposition rate (see Figure 5), while the activation energy of nucleation is decreasing at lower deposition rates. The observed effect may indicate that the deposition rate and temperature affects the concentration of atomic clusters which acts as a precursors of crystalline nucleus. Ongoing investigations suggest the explanation of observed behaviors involve homomolar Te-Te bonds in the films that raises barrier to nucleation [Khoo et al. (2016)]. At the same time, the crystal growth is not affected is not affected by the deposition conditions. The fact that activation energy of growth is not affected by the deposition parameters may explain why samples with the same composition but prepared under different conditions have the same temperature dependence for crystallization while differences in the crystallization rate are still observed [Jeyasingh et al. (2014); Orava et al. (2015)].

In summary, the crystallization kinetics of *GeTe* amorphous films have been studied *in situ* using synchrotron μXRD. The findings provided unique insights,

hitherto little known, due to the obvious difficulties or impractical in conducting *in situ* heating/cooling experiments while simultaneously performing X-ray diffraction in the high enough resolution that it becomes meaningful for advanced microscale (or even submicron and/or nanoscale) phase change memory (PCM) devices. The *in situ* findings revealed that the deposition temperature and rate have significant effects on nucleation of the crystalline phase, but negligible effects on the actual crystal growth. The synchrotron X-ray microdiffraction continues to provide further and deeper insights into the fundamental investigations of crystallization kinetics to enable next generation., (i.e. faster switching) memory devices.

3 Probing Advanced Through-Silicon Via (TSV) Interconnects - Enabling 3D IC (Integrated Circuits) Designs

3D interconnects using though-silicon via (TSV) technology have a potential to improve the performance of microelectronic devices by enabling a design of advanced multi-level chips [Banerjee et al. (2001); Knickerbocker et al. (2005)]. The key point of the design of 3D interconnects using TSV is the control of mechanical stresses in *Cu* TSV and the surrounding *Si* substrate. Stresses in *Cu* TSV introduce a new reliability issues for TSV technology because they may lead to the interconnect breakdown while stresses in *Si* substrate surrounding TSV can affect the electron mobility and hence introduce the keep-away zone where the logical elements cannot be placed [Thompson et al. (2006)].

The annealing conditions and size of TSV are important parameters for TSV based chips fabrication processes [Liao et al. (2013); Sapatnekar (2011)]. In this study we investigate how the annealing conditions and TSV diameter affects the stress state in *Cu* TSV and surrounding *Si*.

Traditional stress measurement techniques like μRaman spectroscopy have a limited use for TSV study because they allow to measure the stress on the surface of *Si* and *Cu* TSV only [Okoro et al. (2008); Liu et al. (2009)]. It is impossible to study the stress distribution inside *Cu* TSV. From the other side, laboratory XRD does not provide sufficient resolution of hydrostatic stress measurement inside *Cu* TSVs [Liu et al. (2009)]. Moreover, it does not allow to find the deviatoric stress components. Hence, synchrotron μXRD is the only tool that can overcome all these issues.

All the TSV test structures used in this study were electroplated at room temperature and annealed after the deposition. The schematic of the cross section of TSV chips is shown on Fig. 6.

The first TSV chip, containing TSVs of 20μm diameters (see [Budiman et al. (2012)] for the details) was used to study the effect of annealing on the stress state inside *Cu* TSV and surrounding *Si*. The sample was further polished along its side as it is shown on Fig. 7. It was done to allow X-ray to penetrate into *Cu* TSV through surrounding *Si* keeping *Si* thick enough to leave the stress state in *Cu* unaffected. Than sample was annealed at 200 during 1hr. The evolution of hydrostatic stress in *Cu* during the annealing was studied *in situ*. The distribution of the deviatoric stress across the cross section of the TSV has been also found after the annealing. In all the cases X-ray beam was focused at the center of TSV perpendicularly to the polished surface as it is illustrated on Fig. 6.

The hydrostatic stress has been found to be compressive before and after annealing (233.8MPa before annealing and 166.6MPa after annealing). The average stress during

the annealing has been found to become tensile (-195.5MPa) which may be the origin of void and crack formation in post-annealed sample (see Fig. 8). The hydrostatic stress after the annealing remains comparable with the stress level in conventional *Cu* interconnect lines [Paik et al. (2006)] and thus can lead to debonding, cracking and voiding which are known for traditional *Cu* lines. The microstructure and deviatoric stress map along TSV cross section is shown on Fig. 9. It demonstrate high average shear stress in *Cu* after annealing which may lead to plastic damages of TSV.

Hence, annealing reduces the hydrostatic stress and cause the void and crack formation inside *Cu* TSV. However, for the annealing parameters used for the study, stress levels still remains high enough to affect the TSV reliability.

Moreover, the hydrostatic stress in *Cu* seems to follow the expansion mismatch between *Cu* and *Si*. The $\Delta\alpha\Delta t$ for *Cu* and *Si* at annealing conditions used during the experiment correspond to a stress difference of about 254MPa. It is close to a stress change during heating and cooling of the sample (430MPa relaxation and 363MPa increase). The difference between observed stress change and the prediction may be associated with *Cu* grain growth during annealing (it make stress more tensile), which is clear from Fig. 8, and plastic deformation that would relax the crystal.

The expansion mismatch should also affect the stress state in *Si* substrate. So, the investigation of the hydrostatic stresses in *Si* surrounding the TSV was done from the top of TSV. The measurement was done in the post-annealed state with TSV cap having only *Cu* TSV with surrounding *Si* (part of *Cu* and solder materials were polished off from the top of the sample). The result is consistent with analytic Lame model as it is shown on Fig. 10 [Lu et al. (2009); Lu et al. (1991)]. It indicates that stress in *Si* is controlled by thermal expansion mismatch between *Cu* and *Si*, hydrostatic stress state in *Cu* (i.e. the "inner pressure" in the "tube" in the Lame model), annealing temperature and *Cu* TSV diameter.

Lame model provide an indication that the diameter of TSV may affect the stress state in *Si* and hence stress in *Cu* TSV. However, stress state in *Cu* TSV is also affected by the intrinsic microstructure evolution in *Cu* during the annealing as we showed earlier. Since the microstructure of electroplated *Cu* may depend on its diameter (grain growth may be constrained at the interface with *Si*), the relation between TSV diameter and stress in *Cu* after annealing is not clear. The study of stress in *Cu* TSV after annealing for different TSV diameters is presented below.

The samples of three different diameter of 2μm, 5μm and 8μm were used in the study. TSV for all three samples were annealed at 100 after deposition, polished from the top, annealed at 400 and polished from the top again. Only post-annealed state of the samples was studied. The experimental procedure was the same as the one used to study stress state in *Cu* for the first sample (20μm diameter).

The results clearly demonstrate that deviatoric stress is increasing with decrease of diameter of TSV (see Fig. Error: Reference source not found. The hydrostatic stresses in *Cu* were found to be 443MPa for 8μm sample, 354MPa for 5μm sample and 408MPa for 8μm sample. The hydrostatic stress for 5μm and 8μm TSVs follow the trend predicted by Lame model (stress increases with TSV diameter), however stress in 2μm TSV appeared to be the highest. We speculate that stress for small diameters may be mainly controlled by microstructure evolution in *Cu* during the annealing. It is also consistent with deviatoric stress behavior. However, at the larger diameters of TSV the contribution of thermal expansion difference play the main role.

In summary, stress state of *Cu* TSVs and surrounding *Si* substrate was studied. It was found that stress state in *Cu* TSV is controlled by annealing temperature, thermal expansion coefficient mismatch between *Cu* and *Si*, TSV diameter and its

microstructure. At small diameters the stress is controlled by microstructure evolution during annealing. At larger diameters the stress is controlled by the thermal mismatch between *Cu* and *Si*.

4 Microstructural Evaluation of the Solder Joint of a Crystalline Silicon Solar Cell String after Thermal Cycling

Solder joint cracking is one of the major failure mechanisms in microelectronic packages and crystalline silicon photovoltaic modules [Steinberg (2001)-Wendt et al. (2009)]. Though thermo-mechanical loading is the major cause of the solder cracks, it was also noticed that formation of non-eutectic intermetallic compounds in the solder may trigger premature cracking even at low loads [Pang et al. (2001)]. In this scenario, study of the microstructure of the solder joint before and after thermal cycling would become an essential step to understand the effect of thermal cycling on the microstructural evolution of the solder joint [Pang et al. (2001)-Kim et al. (2010)]. In general microstructure studies will be done using imaging methods such as SEM. Though these methods successfully show the presence of different intermetallic compounds, they cannot exactly identify the compounds and the analysis would be based on appearance of the image and lot speculation goes into the final conclusion. More advanced technique such as EDX can only give the composition of elements present at a location. On the other hand a normal laboratory XRD machine may not be able to show these compounds as they me be preset in traces, which is beyond the resolution of the low resolution laboratory X-ray beam (size 100 μm).

As already explained in the preceding sections, Synchrotron X-ray micro-diffraction is equipped with a high energy beam of energy 5 -25 keV and beam size < 1 μm and a 2D detector [Tamura (2014)]. With this specialized capability, the setup can detect even trace amount compounds effectively and it is possible to identify the particular intermetallic compound present in the solder joint. When a polycrystalline sample is subjected to monochromatic micro X-ray beam, it generates the Debye-Scherer ring patterns or powder diffraction patterns [Budiman et al. (2014)], indexing these patterns will unfold the information of the particular intermetallic compound present in the sample. Microstructure analysis of a typical solder joint of crystalline silicon solar cell using Synchrotron Micro X-ray Diffraction [Budiman et al. (2014)] was presented here as an example to demonstrate the capability of this powerful technique and its applicability to the area of microstructure evaluation. The analyzed solder joint specimen was made of typical back contact crystalline silicon solar cells, manufactured by Sunpower corporation, CA, USA and the bus bar was made of tin coated copper ribbon (Fig. 12). The cells and the bus bar are joined by solder joints made of typical *Sn-Ag* family solders (melting point at 217 - 220 C) as shown in Figure 12. The solder joint assembly was carefully cast in an epoxy mould and a section was diced as shown in Figure 13 (section A-A of Figure 12) and polished to enable X-ray diffraction of the joint cross section. The solder joint was of area few sq. mm and the thickness is of the order of tens of microns. Typical grain size of the solder joint material is around 0.5 - 15 μm. The solder joint sample was thermally cycled from -40 C to 150 C for 2000 cycles and the XRD experiment was conducted before and after cycling.

Figure 13 show the powder diffraction pattern obtained from the sectioned solder joint sample. The zoomed in plot in Figure 13 clearly show the indexed Debye-Scherer

ring patterns clearly indicate presence of intermetallic compound , after thermal cycling due to activated inter-diffusion of *Cu* and *Sn*. This intermetallic compound is stiffer and brittle than the bulk solder and it could make the solder joint brittle and eventually lead to cracking even at lower loads than expected. [Mei et al. (2005); Kim et al. (2010)]. This observation of the brittle intermetallic phase may not have been possible without the high-energy Synchrotron X-ray beam of submicron size. Further the Synchrotron X-ray Micro-diffraction can also be used to evaluate the residual stress in the crystalline silicon solar cells even after encapsulation. Detailed explanation on this account is beyond scope of this paper but more information and details can be obtained from references [Budiman et al. (2014); Rengarajan et al. (2016); Tippabhotla et al. (2016); Culity and Stock (1978)].

Simple ex-situ microstructural evaluation of the solar PV solder joint to identify intermetallic compounds was demonstrated in this manuscript. The powder diffraction patterns indicate formation of brittle intermetallic phase in the solder joint upon thermal cycling due to activated inter diffusion of *Cu* and *Sn*. This technique can be further extended to perform a more interesting in-situ investigations to demonstrate the evolution of the intermetallic phase during the thermal cycling of the joint and associated stress evolution can be quantified to optimize the solder joint materials/processes and designs.

5 Conclusions

To be done

Acknowledgements: The Advanced Light Source (ALS) is supported by the Director, Office of Science, Office of Basic Energy Sciences, of the U.S. Department of Energy under Contract No. DE-AC02-05CH11231 at the Lawrence Berkeley National Laboratory (LBNL).

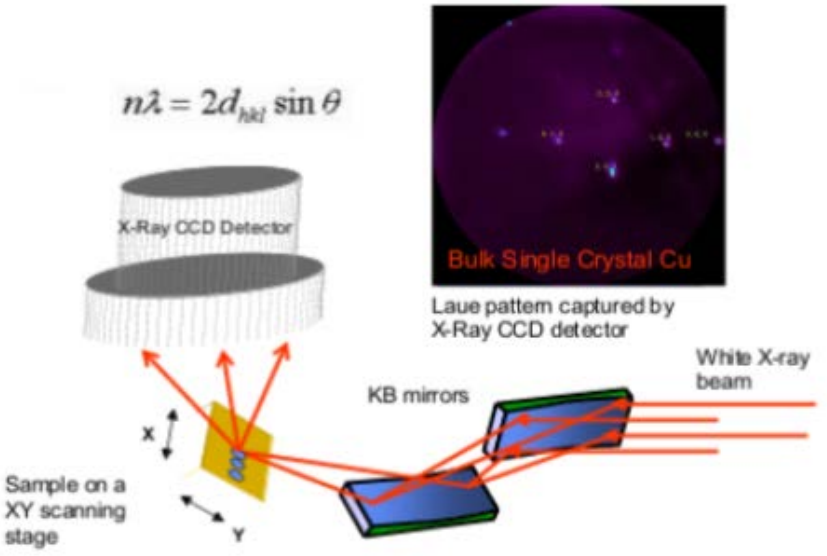

Figure 1: Schematic of Synchrotron X-ray Micro-diffraction setup.

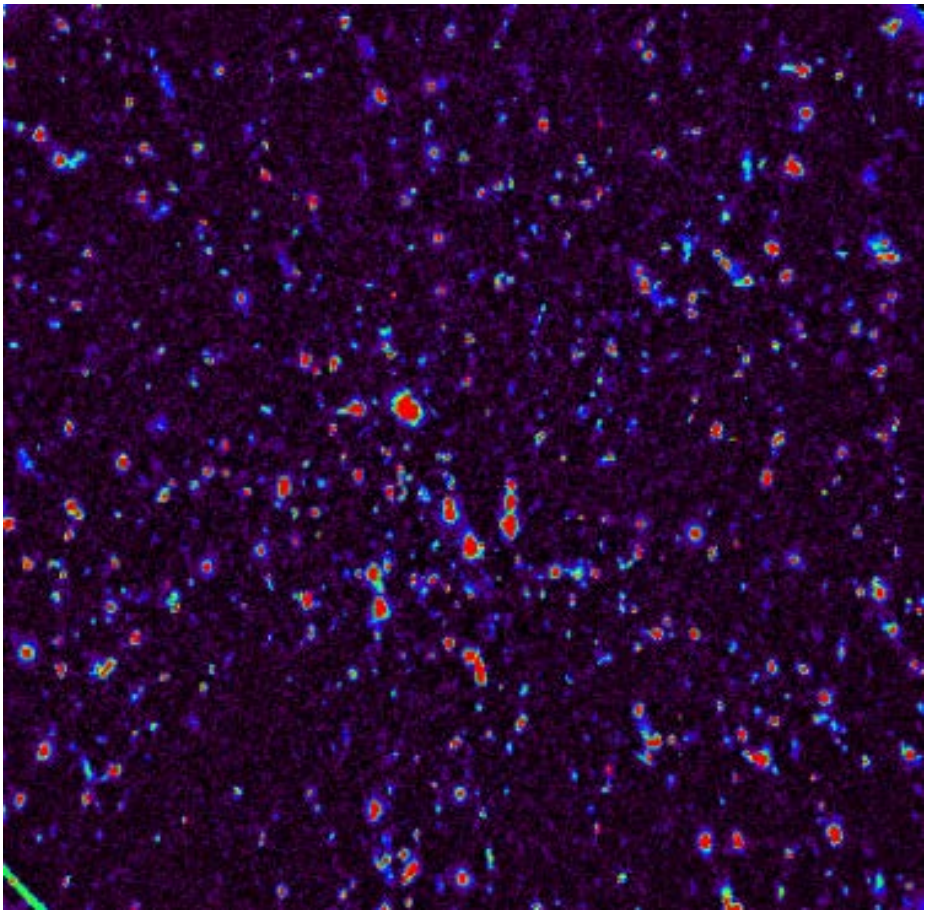

Figure 2: Laue diffraction pattern of a polycrystalline sample.

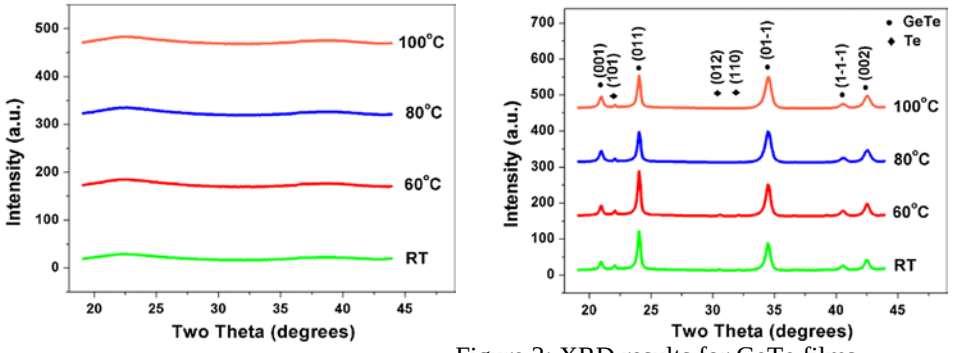

Figure 3: XRD results for GeTe films.
(a) As-deposited and (b) fully crystallized at 230 °C.

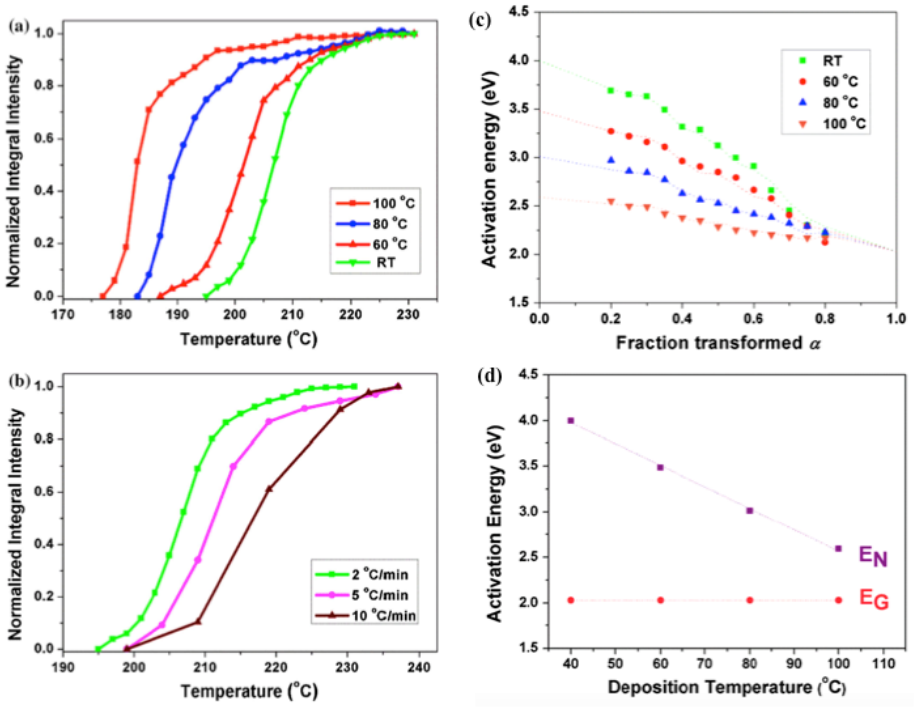

Figure 4: (a) Transformation curves for GeTe films deposited at different temperatures, based on normalized magnitudes of the (011) peak observed at 230 Â°C. The heating rate was 2 Â°C/min. (b) Transformation curves for GeTe films deposited at room temperature and heated at different rates. (c) The local effective activation energy Ec as a function of the fraction transformed a for films prepared at various deposition temperatures and (d) activation energies for nucleation and growth as a function of the deposition temperature.

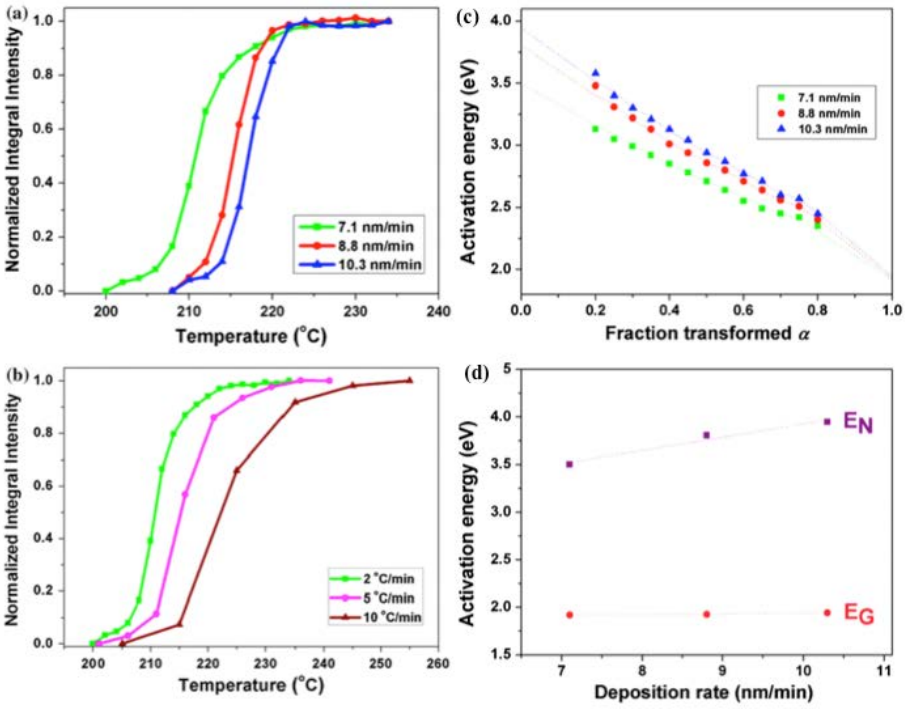

Figure 5: (a) Transformation curves for GeTe films deposited at different deposition rates, normalized by the magnitude of the (011) peak observed at 235 Â°C, with a heating rate of 2 Â°C/min. (b) transformation curves for GeTe films deposited at a rate of 7.1 nm/min and heated at different rates. (c) The local effective activation energy Ec as a function of the fraction transformed a for films prepared at various deposition rates and (d) activation energies for nucleation and growth as a function of the deposition rate.

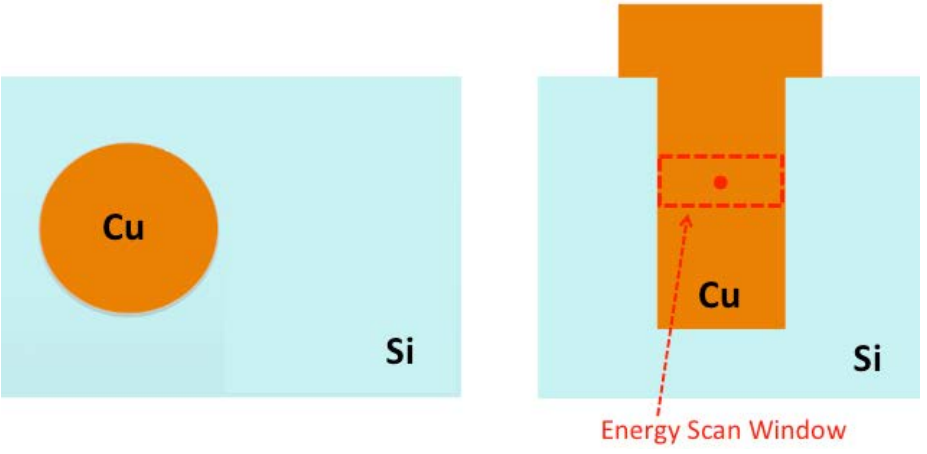

Figure 6: Schematic of TSV showing the Energy Scan Region for Evaluating Hydrostatic Stress: top view (left) and cross section view (right).

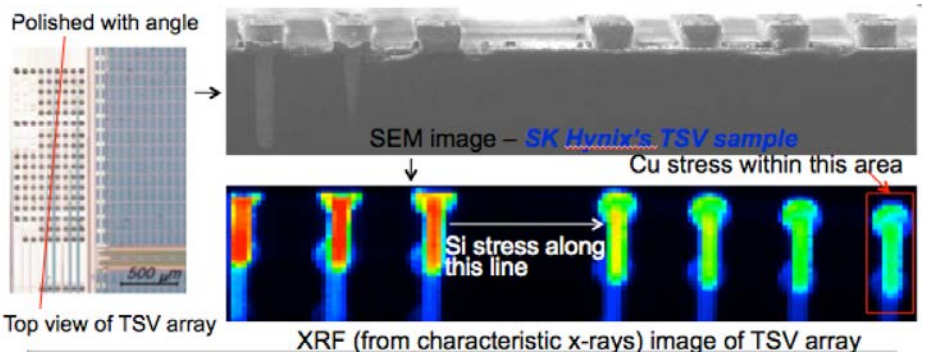

Figure 7: TSV Sample, Polished Section and Associated XRF Image Showing TSVs.

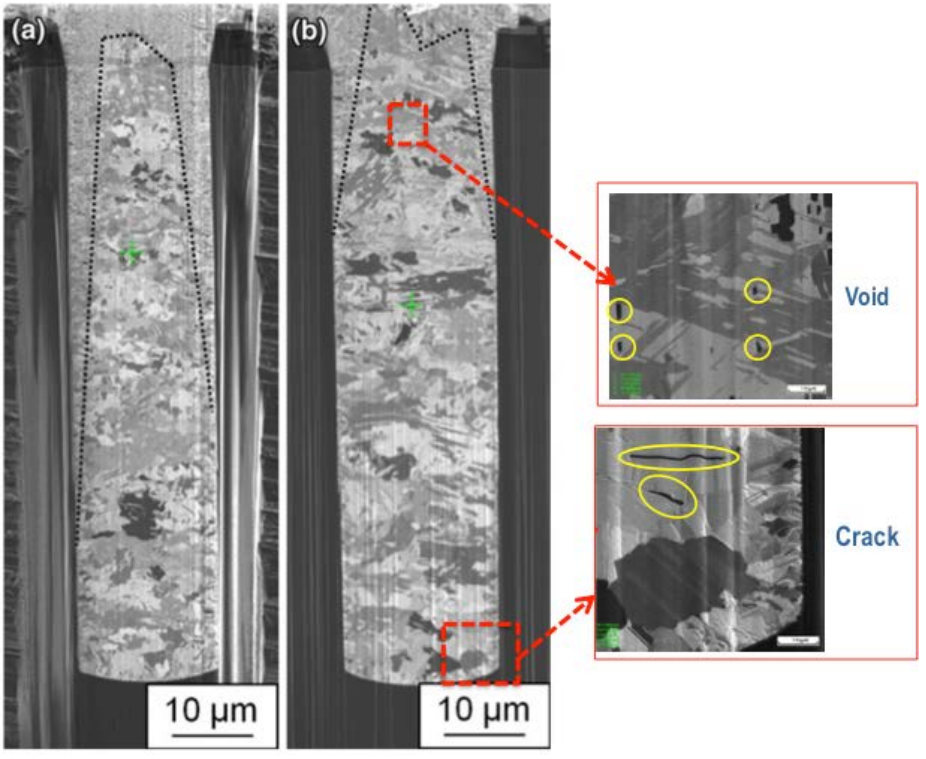

Figure 8: FIB images of the TSV (a) before annealing and (b) after annealing at 200C for 1hr. The small-grain area and the large-grain areas are indicated by the dotted line. Cracks and Voids formed after annealing are shown in (b).

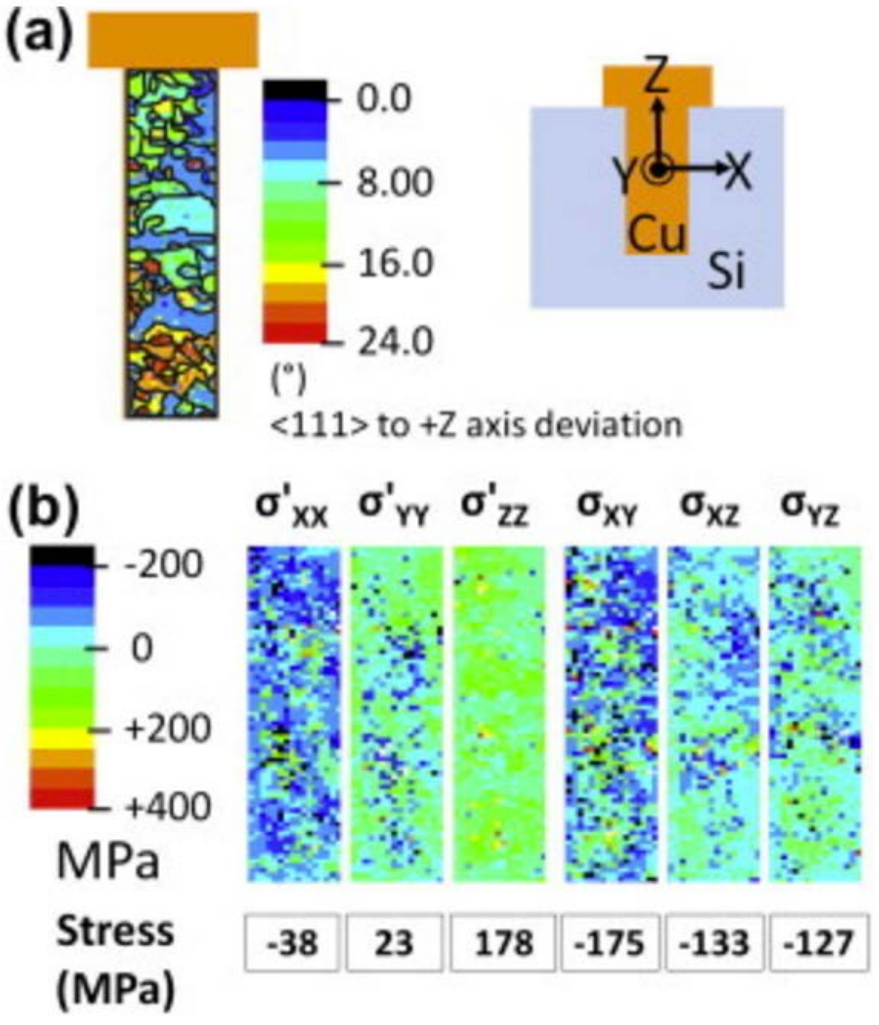

Figure 9: Laue Diffraction results showing (a) the grain orientation map, (b) the deviatoric stress in the Cu TSV sample in the post-annealed state (after annealing at 200Â Â°C for 1Â h). The XYZ coordinates used here are as described in (a) with respect to the laboratory coordinates. All the stress values on the figure are the average stress of all the stresses from each pixel (1μm step size in X and Y directions) in the measured area of TSV.

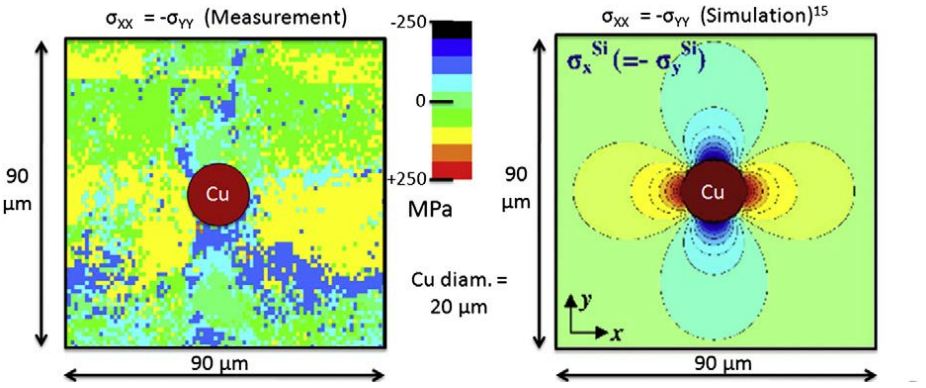

Figure 10: Si stress state surrounding the Cu TSV showing the measured stress map from the top of the TSV sample (left) and analytic simulation result performed by other research group [Lu et al. (2009)] (right).

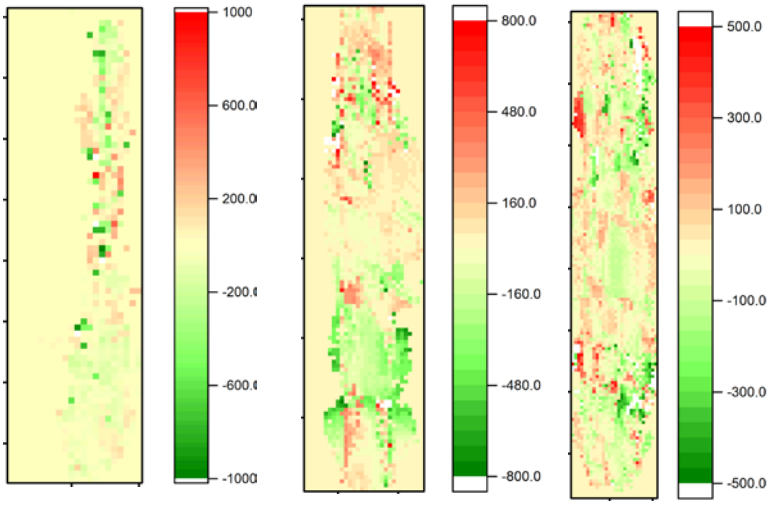

Figure 11: Deviatoric stress () distribution across the *Cu* TSV after annealing for different diameters. The pixel sizes and coordinate system used here are the same as in Fig. 9.

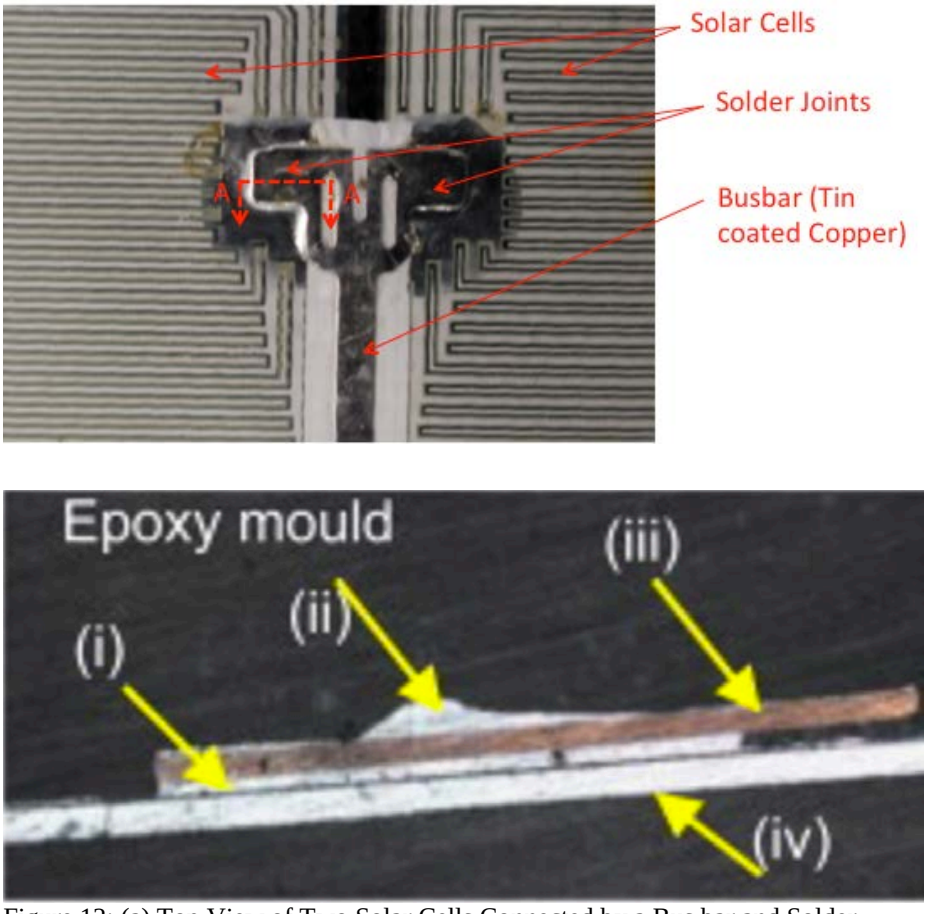

Figure 12: (a) Top View of Two Solar Cells Connected by a Bus bar and Solder Joints, (b) Cross Section of the Solder Joint Cast in Epoxy Mould Showing (i) Solder Joint between Cell and Bus bar, (ii) Residual Solder Lump on the Bus bar, (iii) Bus bar and (iv) Silicon Solar Cell, for X-ray.

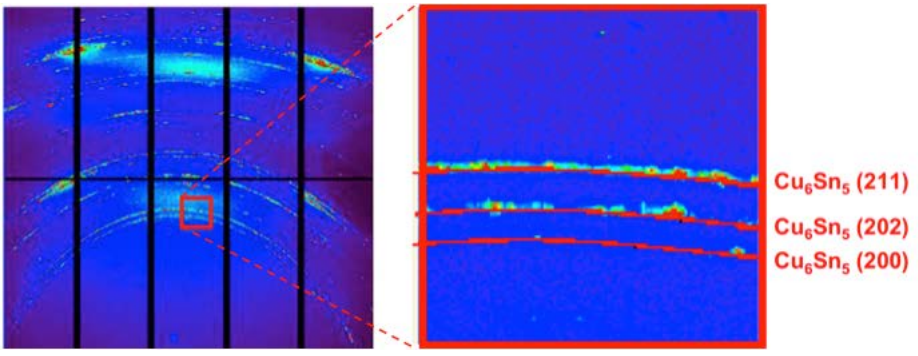

Figure 13: Indexed Powder Diffraction Pattern of the Solder Joint Sample.

References

1. N Tamura, M Kunz, K Chen, RS Celestre, AA MacDowell, and T Warwick. A superbend x-ray microdiffraction beamline at the advanced light source. *Materials Science and Engineering: A*, 524 (1): 28–32, 2009.
2. Nobumichi Tamura. XMAS: a versatile tool for analyzing synchrotron x-ray microdiffraction data. *Strain and Dislocation Gradients from Diffraction. Spatially Resolved Local Structure and Defects*, pages 125–155, 2014.
3. AS Budiman, PR Besser, CS Hau-Riege, A Marathe, Y-C Joo, N Tamura, JR Patel, and WD Nix. Electromigration-induced plasticity: Texture correlation and implications for reliability assessment. *Journal of electronic materials*, 38 (3): 379–391, 2009.
4. AS Budiman, G Illya, V Handara, WA Caldwell, C Bonelli, M Kunz, N Tamura, and D Verstraeten. Enabling thin silicon technologies for next generation c-si solar pv renewable energy systems using synchrotron x-ray microdiffraction as stress and crack mechanism probe. *Solar Energy Materials and Solar Cells*, 130: 303–308, 2014.
5. A.S. Budiman, H.-A.-S. Shin, B.-J. Kim, S.-H. Hwang, H.-Y. Son, M.-S. Suh, Q.-H. Chung, K.-Y. Byun, N. Tamura, M. Kunz, and Y.-C. Joo. Measurement of stresses in cu and si around through-silicon via by synchrotron x-ray microdiffraction for 3-dimensional integrated circuits. *Microelectronics Reliability*, 52 (3): 530 – 533, 2012a. ISSN 0026-2714.
6. A. S. Budiman, W. D. Nix, N. Tamura, B. C. Valek, K. Gadre, J. Maiz, R. Spolenak, and J. R. Patel. Crystal plasticity in cu damascene interconnect lines undergoing electromigration as revealed by synchrotron x-ray microdiffraction. *Applied Physics Letters*, 88 (23): 233515, 2006.
7. Yingxia Liu, Nobumichi Tamura, Dong Wook Kim, Sam Gu, and KN Tu. A metastable phase of tin in 3d integrated circuit solder microbumps. *Scripta Materialia*, 102: 39–42, 2015.
8. Kai Chen, N Tamura, BC Valek, and KN Tu. Plastic deformation in al (cu) interconnects stressed by electromigration and studied by synchrotron polychromatic x-ray microdiffraction. *Journal of Applied Physics*, 104 (1): 013513, 2008.
9. Arief Suriadi Budiman, Seung-Min Han, Nan Li, Qiang-Min Wei, Patricia Dickerson, Nobumichi Tamura, Martin Kunz, and Amit Misra. Plasticity in the nanoscale cu/nb single-crystal multilayers as revealed by synchrotron laue x-ray microdiffraction. *J. Mater. Res.*, 10, 2012b.
10. AS Budiman, Karthic R Narayanan, N Li, J Wang, N Tamura, M Kunz, and A Misra. Plasticity evolution in nanoscale cu/nb single-crystal multilayers as revealed by synchrotron x-ray microdiffraction. *Materials Science and Engineering: A*, 635: 6–12, 2015.
11. Karthic Narayanan Rengarajan, Ihor Radchenko, Gregoria Illya, Vincent Handara, Martin Kunz, Nobumichi Tamura, and Arief Suriadi Budiman. Low stress encapsulants? influence of encapsulation materials on stress and fracture of thin silicon solar cells as revealed by synchrotron x-ray submicron diffraction. *Procedia Engineering*, 139: 76–86, 2016.
12. Sasi Kumar Tippabhotla, Ihor Radchenko, Karthic Narayanan Rengarajan, Gregoria Illya, Vincent Handara, Martin Kunz, Nobumichi Tamura, and Arief Suriadi Budiman. Synchrotron x-ray micro-diffraction–probing stress

state in encapsulated thin silicon solar cells. *Procedia Engineering*, 139: 123–133, 2016.
13. AV Kolobov, P Fons, and J Tominaga. Phase-change optical recording: Past, present, future. *Thin Solid Films*, 515 (19): 7534–7537, 2007.
14. Wojciech WeŃnic and Matthias Wuttig. Reversible switching in phase-change materials. *Materials today*, 11 (6): 20–27, 2008.
15. Alexander V Kolobov, Paul Fons, Anatoly I Frenkel, Alexei L Ankudinov, Junji Tominaga, and Tomoya Uruga. Understanding the phase-change mechanism of rewritable optical media. *Nature materials*, 3 (10): 703–708, 2004.
16. Matthias Wuttig and Noboru Yamada. Phase-change materials for rewriteable data storage. *Nature materials*, 6 (11): 824–832, 2007.
17. Dominic Lencer, Martin Salinga, Blazej Grabowski, Tilmann Hickel, Jörg Neugebauer, and Matthias Wuttig. A map for phase-change materials. *Nature Materials*, 7 (12): 972–977, 2008.
18. Simone Raoux and Daniele Ielmini. Phase change materials and their application to nonvolatile memories. *Chemical reviews*, 110 (1): 240–267, 2009.
19. Dominic Lencer, Martin Salinga, and Matthias Wuttig. Design rules for phase-change materials in data storage applications. *Advanced Materials*, 23 (18): 2030–2058, 2011.
20. Y Sutou, T Kamada, M Sumiya, Y Saito, and J Koike. Crystallization process and thermal stability of ge 1 cu 2 te 3 amorphous thin films for use as phase change materials. *Acta Materialia*, 60 (3): 872–880, 2012.
21. Roman Svoboda and Jiří Málek. Interpretation of crystallization kinetics results provided by dsc. *Thermochimica Acta*, 526 (1): 237–251, 2011.
22. Chee Ying Khoo, Hai Liu, Wardhana A Sasangka, Riko I Made, Nobu Tamura, Martin Kunz, Arief S Budiman, Chee Lip Gan, and Carl V Thompson. Impact of deposition conditions on the crystallization kinetics of amorphous gete films. *Journal of Materials Science*, 51 (4): 1864–1872, 2016.
23. Homer E Kissinger. Reaction kinetics in differential thermal analysis. *Analytical chemistry*, 29 (11): 1702–1706, 1957.
24. Rakesh Jeyasingh, Scott W Fong, Jaeho Lee, Zijian Li, Kuo-Wei Chang, Davide Mantegazza, Mehdi Asheghi, Kenneth E Goodson, and H-S Philip Wong. Ultrafast characterization of phase-change material crystallization properties in the melt-quenched amorphous phase. *Nano letters*, 14 (6): 3419–3426, 2014.
25. Jiri Orava, Daniel W Hewak, and A Lindsay Greer. Fragile-to-strong crossover in supercooled liquid ag-in-sb-te studied by ultrafast calorimetry. *Advanced Functional Materials*, 25 (30): 4851–4858, 2015.
26. Kaustav Banerjee, Shukri J Souri, Pawan Kapur, and Krishna C Saraswat. 3-d ics: A novel chip design for improving deep-submicrometer interconnect performance and systems-on-chip integration. *Proceedings of the IEEE*, 89 (5): 602–633, 2001.
27. John U Knickerbocker, Paul S Andry, L Paivikki Buchwalter, Alina Deutsch, Raymond R Horton, Keith A Jenkins, Young Hoon Kwark, Gerald McVicker, Chirag S Patel, Robert J Polastre, et al. Development of next-generation system-on-package (sop) technology based on silicon carriers with fine-pitch chip interconnection. *IBM Journal of Research and Development*, 49 (4.5): 725–753, 2005.

28. Scott E Thompson, Guangyu Sun, Youn Sung Choi, and Toshikazu Nishida. Uniaxial-process-induced strained-si: extending the cmos roadmap. *IEEE Transactions on Electron Devices*, 53 (5): 1010–1020, 2006.
29. Ming-Han Liao, M-Y Yu, G-H Liu, C-H Chen, and T-K Hsu. The demonstration of nonlinear analytic model for the strain field induced by thermal copper filled tsvs (through silicon via). *AIP Advances*, 3 (8): 082123, 2013.
30. Sachin S Sapatnekar. Overcoming variations in nanometer-scale technologies. *Emerging and Selected Topics in Circuits and Systems, IEEE Journal on*, 1 (1): 5–18, 2011.
31. Chukwudi Okoro, Yu Yang, Bart Vandevelde, Bart Swinnen, Dirk Vandepitte, Bert Verlinden, and Ingrid De Wolf. Extraction of the appropriate material property for realistic modeling of through-silicon-vias using μ-raman spectroscopy. In *Interconnect Technology Conference, 2008. IITC 2008. International*, pages 16–18. IEEE, 2008.
32. Xi Liu, Qiao Chen, Pradeep Dixit, Ritwik Chatterjee, Rao R Tummala, and Suresh K Sitaraman. Failure mechanisms and optimum design for electroplated copper through-silicon vias (tsv). In *Electronic Components and Technology Conference, 2009. ECTC 2009. 59th*, pages 624–629. IEEE, 2009.
33. Jong-Min Paik, Il-Mok Park, and Young-Chang Joo. Effect of grain growth stress and stress gradient on stress-induced voiding in damascene cu/low-k interconnects for ulsi. *Thin solid films*, 504 (1): 284–287, 2006.
34. Kuan H Lu, Xuefeng Zhang, Suk-Kyu Ryu, Jay Im, Rui Huang, and Paul S Ho. Thermo-mechanical reliability of 3-d ics containing through silicon vias. In *Electronic Components and Technology Conference, 2009. ECTC 2009. 59th*, pages 630–634. IEEE, 2009.
35. TC Lu, J Yang, Z Suo, AG Evans, R Hecht, and R Mehrabian. Matrix cracking in intermetallic composites caused by thermal expansion mismatch. *Acta metallurgica et materialia*, 39 (8): 1883–1890, 1991.
36. Dave S Steinberg. *Preventing thermal cycling and vibration failures in electronic equipment*. Wiley-Interscience, 2001.
37. Andrew M Gabor, Mike Ralli, Shaun Montminy, Luis Alegria, Chris Bordonaro, Joe Woods, Larry Felton, Max Davis, Brian Atchley, and Tyler Williams. Soldering induced damage to thin si solar cells and detection of cracked cells in modules. In *21st European Photovoltaic Solar Energy Conference, Dresden, Germany, September*, pages 4–8, 2006.
38. J Wendt, M Träger, M Mette, A Pfennig, and B Jäckel. The link between mechanical stress induced by soldering and micro damages in silicon solar cells. *Proc. of 24th EUPVSEC*, pages 3420–3423, 2009.
39. HLJ Pang, KH Tan, XQ Shi, and ZP Wang. Microstructure and intermetallic growth effects on shear and fatigue strength of solder joints subjected to thermal cycling aging. *Materials Science and Engineering: A*, 307 (1): 42–50, 2001.
40. John HL Pang, TH Low, BS Xiong, Xu Luhua, and CC Neo. Thermal cycling aging effects on sn–ag–cu solder joint microstructure, imc and strength. *Thin Solid Films*, 462: 370–375, 2004.
41. Zequn Mei, Mudasir Ahmad, Mason Hu, and Gnyaneshwar Ramakrishna. Kirkendall voids at cu/solder interface and their effects on solder joint

reliability. In *Electronic Components and Technology Conference, 2005. Proceedings. 55th*, pages 415–420. IEEE, 2005.
42. Byoung-Joon Kim, Gi-Tae Lim, Jaedong Kim, Kiwook Lee, Young-Bae Park, Ho-Young Lee, and Young-Chang Joo. Intermetallic compound growth and reliability of cu pillar bumps under current stressing. *Journal of electronic materials*, 39 (10): 2281–2285, 2010.
43. BD Culity and SR Stock. Elements of x-ray diffraction. *2nd, Addition-Wesley, MA, London*, 1978.